JACS
JOURNAL OF THE AMERICAN CHEMICAL SOCIETY
Communication
pubs.acs.org/JACS

Molecularly Imprinted Polymer-Based Catalytic Micromotors for Selective Protein Transport

Jahir Orozco, Allan Cortés, Guanzhi Cheng, Sirilak Sattayasamitsathit, Wei Gao, Xiaomiao Feng, Yufeng Shen, and Joseph Wang*

Department of Nanoengineering, University of California, San Diego, La Jolla, California 92093, United States

Supporting Information

ABSTRACT: We demonstrate an attractive nanomachine "capture and transport" target isolation strategy based on molecularly imprinted polymers (MIPs). MIP-based catalytic microtubular engines are prepared by electropolymerization of the outer polymeric layer in the presence of the target analyte (template). Tailor-made selective artificial recognition sites are thus introduced into the tubular microtransporters through complementary nanocavities in the outer polymeric layer. The new microtransporter concept is illustrated using bilayer poly(3,4-ethylenedioxythiophene) (PEDOT)/Pt−Ni microengines and fluorescein isothiocyanate (FITC)-labeled avidin (Av-FITC) as the template. The avidin-imprinted polymeric layer selectively concentrates the fluorescent-tagged protein target onto the moving microengine without the need for additional external functionalization, allowing "on-the-fly" extraction and isolation of Av-FITC from raw serum and saliva samples along with real-time visualization of the protein loading and transport. The new micromachine−MIP-based target isolation strategy can be extended to the capture and transport of other important target molecules, leading toward diverse biomedical and environmental applications.

Recent progress in the field of synthetic nanomachines has opened the door to new and important applications.[1−3] For example, active transport by receptor-functionalized artificial nanomotors propelled in complex samples offers an attractive strategy for isolating target analytes[4−6] in a manner analogous to transport processes by protein motors.[7,8] In particular, autonomously moving, chemically powered tubular microengines functionalized with different bioreceptors (e.g., oligonucleotides, antibodies) have been shown to be extremely useful for "on-the-fly" recognition and transport of a wide array of biological targets, ranging from nucleic acids to proteins and cancer cells.[6,9−11] Such nanomachine-driven target isolation and transport capability of receptor-modified microtransporters holds considerable promise for diverse biomedical and environmental applications.

Here we present a new nanomachine-based separation concept that relies on molecularly imprinted artificial recognition cavities. Molecularly imprinted polymers (MIPs) containing selective recognition sites[12] have attracted considerable interest in a variety of sensor and separation applications because of their high specificity, ease of preparation, and thermal and chemical stability.[13−15] Such specific artificial recognition cavities are introduced within the polymeric matrix via polymerization around the analyte (template) molecule followed by removal of the print template, leaving behind complementary binding sites. The resulting matrices offer selective binding and can exert antibody-like affinities toward the target substances.[15b] In this report, we show that molecular imprinting allows cost-effective preparation of tailor-made self-propelled microtransporters with predetermined specificity for selective "on-the-fly" isolation of target substances. Unlike bioreceptor-functionalized motors, the recognition properties of the imprinted synthetic polymers can withstand harsher conditions than their natural counterparts, including high temperature and pressure, extreme pH, and organic solvents,[12c] making the new MIP-based nanomachines attractive for diverse practical applications. Similarly, the presence of the hydrogen peroxide fuel, which could affect bioreceptor stability and biorecognition events, has no effect upon the operation of the MIP micromotors.

To illustrate the new nanomachine−MIP "capture and transport" concept, we designed tubular microtransporters with cavity binding sites for fluorescein isothiocyanate (FITC)-labeled avidin (Av-FITC) within their outer polymeric layer. The imprinted recognition sites for the target protein template were introduced onto the nanomachine surface during the electropolymerization of the outer poly(3,4-ethylenedioxythiophene) (PEDOT) layer. Electropolymerization has been widely used to prepare molecularly imprinted recognition cavities for a variety of optical and electrochemical biosensors.[13b,16] Gyurcsányi and colleagues recently reported the preparation of avidin-imprinted PEDOT nanorods and films doped with poly(styrenesulfonate) (PSS) for label-free surface plasmon resonance (SPR) sensing of proteins.[17] The PEDOT/PSS complex is ideally suited for imprinting of protein targets because of its ability to generate the necessary hydrogen bonds and electrostatic and $\pi-\pi$ interactions (Figure 1b).[17a] The outer tubular PEDOT layer of our microengine was grown on the inner walls of the micropores of a polycarbonate membrane containing the preadsorbed Av-FITC template. The electropolymerization of the outer layer was followed by electrodeposition of the inner Ni and Pt metallic layers (for magnetic guidance and generation of the oxygen-bubble propulsion thrust, respectively) and dissolution of the membrane and concomitant removal of the protein template. A scanning

Received: February 20, 2013
Published: March 26, 2013

   dx.doi.org/10.1021/ja4018545 | J. Am. Chem. Soc. 2013, 135, 5336−5339

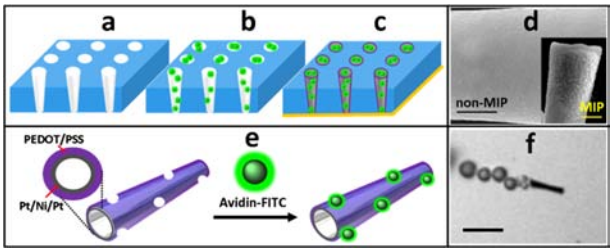

Figure 1. Preparation and characterization of the MIP-based micromotor and the strategy for capture and transport of the target protein. (a–c) To fabricate the template-imprinted microtubes, a dry hydrophobic sacrificial polycarbonate membrane (a) adsorbs the positively charged protein template by electrostatic interaction (b); after sputtering of a conductive Au layer, sequential deposition is used to deposit the PEDOT, Pt, Ni, and Pt layers (c). The resulting PEDOT–Pt–Ni–Pt multilayer microtubes are released from the membrane by immersion in an organic solvent that also removes the template protein, leaving imprinted nanocavities on the outermost surface of the micromotor. (d) SEM images showing the surfaces of a control non-MIP micromotor and (inset) the MIP-based micromotor. Scale bar = 500 nm. (e) Scheme illustrating the capture of the fluorescent-tagged target protein by the self-propelled MIP microengines. (f) Image illustrating the bubble-propelled MIP micromotor in a PBS solution containing 0.75% H_2O_2. Scale bar = 20 μm.

electron microscopy (SEM) image of the MIP-based micromotor (Figure 1d inset) indicated a highly rough outermost polymeric surface, reflecting the large number of exposed complementary imprinted cavities. In contrast, a much smoother surface was observed (in Figure 1d) for the non-MIP micromotor. The essential conical shape of the microtube was retained following the imprinting process.

As will be demonstrated below, the micromachine-based MIP-isolation concept relies on selective and efficient "on-the-fly" binding of the fluorescent-tagged protein to the cavity recognition sites (Figure 1e). The outer polymeric layer thus possesses "built-in" recognition properties, eliminating the need for additional receptor functionalization steps. Autonomous movement of the template-imprinted microtransporter in the sample mixture results in selective loading of the target protein along with effective discrimination against nontarget proteins. Direct extraction and isolation of Av-FITC from raw serum and saliva samples can thus be accomplished following short navigation times. Video 1 in the Supporting Information (SI) and Figure 1f show a template-imprinted microengine moving rapidly (247 ± 11 μm/s) in the presence of a low fuel level (0.75% H_2O_2 containing 1.25% sodium cholate). The non-MIP counterpart moved at 241 ± 12 μm/s under the same conditions. Apparently, introduction of the MIP-recognition cavities had no effect upon the efficient propulsion behavior characteristic of polymer/Pt microtube engines. As indicated in SI video 1, the MIP microengine moves in a straight line while releasing from its wider opening a distinct oxygen bubble trail generated by catalytic oxidation of its H_2O_2 fuel at the inner Pt layer. Much lower speeds of 34.8 ± 4.2 and 29.6 ± 0.3 μm/s were observed for the magnetically guided MIP and non-MIP micromotors containing an intermediate Ni layer, respectively, as expected for Ni-containing polymer-based microtubular engines.[18]

The resulting template-imprinted microengines offer direct target recognition, capture, and transport, and the fluorescent FITC tag of the target protein provides real-time optical visualization of the MIP–avidin binding event based on changes in the fluorescence intensity. For example, the optical image in Figure 2a and the corresponding video (SI video 2) indicate that a short navigation time of 14 min in the 0.25 mg/mL target protein solution yielded complete fluorescent coverage of the microengine surface. These data, along with the subsequent control experiments discussed below, confirmed the presence of the complementary surface recognition sites, in accordance with early work on nonmotor nanorods,[17a] and indicated again that the template imprinting does not compromise the efficient bubble propulsion. In agreement with early work,[10] the protein solution led to a lower speed (16.6 ± 1.3 μm/s). As will be illustrated below, the target recognition was coupled with effective discrimination against coexisting compounds.

Different negative controls were used to evaluate the binding specificity of the protein-imprinted microtubes toward the target protein, avidin (Figure 2b,c). For example, a non-MIP micromotor was prepared using similar conditions as the MIP-based motor but without the preadsorbed Av-FITC protein template. The optical microscopy image obtained with the non-MIP PEDOT/PSS micromotor (Figure 2b) shows no apparent binding of the protein, despite its higher concentration and the longer navigation time. Similarly, no capture of the target protein was observed using a conventional microengine[18] based on the anionic surfactant sodium dodecyl sulfate (SDS) instead of the PSS polyanion (Figure 2c), partially reflecting the SDS-induced denaturation of the protein, which affects the 3D MIP–protein structure. Specific binding is a key requirement for the new MIP-based nanomotor isolation platform. The avidin-imprinted PEDOT/PSS microtransporters were shown to discriminate against functional homologues of avidin, such as

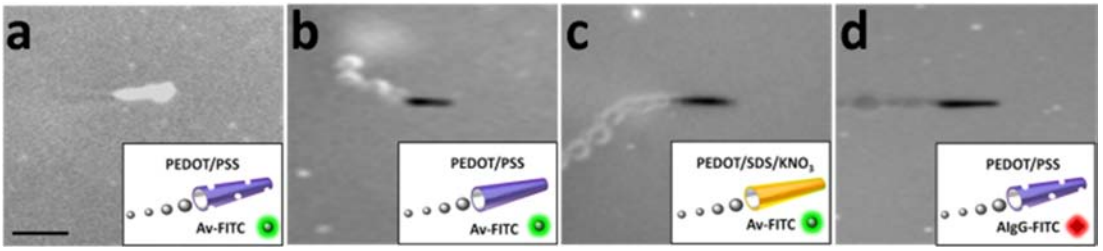

Figure 2. Specificity of the "capture and transport" process of the template-imprinted microengines: (a) Time-lapse image taken after the MIP-based micromotor had navigated for 14 min in the 0.25 mg/mL Av-FITC target protein solution (see SI video 2). (b–d) Control experiments involving navigation for 20 min: (b, c) non-MIP micromotors with (b) PSS and (c) SDS as counterions in a 0.5 mg/mL Av-FITC target protein solution; (d) MIP-based micromotor with PSS counterion moving in a solution containing the nontarget AIgG-FITC (0.5 mg/mL). Conditions were the same as in Figure 1. Scale bar = 20 μm.

dx.doi.org/10.1021/ja4018545 | J. Am. Chem. Soc. 2013, 135, 5336–5339

FITC-labeled anti-immunoglobulin G (AIgG-FITC).[17b] No binding and transport were observed following movement of the MIP-based PEDOT/PSS micromotor for 20 min in a phosphate buffer solution containing the nontarget protein AIgG-FITC (0.5 mg/mL) (Figure 2d). The corresponding real-time videos (included in SI video 2) clearly illustrate the specificity of the MIP–PEDOT/PSS microtransporter, the negligible nonspecific adsorption onto the PEDOT/PSS outer polymer, and the crucial role of the MIP recognition sites in attaining such efficient and selective uptake of the target protein onto the moving machine.

The imprinted polymeric layer selectively concentrates the fluorescent-tagged target protein onto the moving microengine. Such enrichment is illustrated in Figure 3A(a–e) and SI video

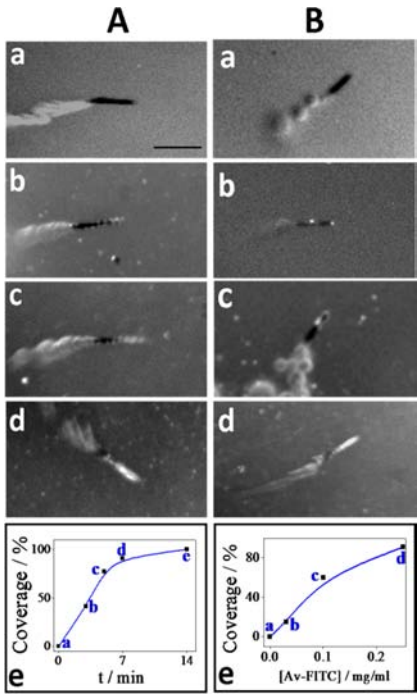

Figure 3. Dependence of protein uptake by the MIP-based micromotor on (A) the locomotion time and (B) the target concentration. (A) (a–d) Time-lapse images, each taken over a 3 s period, after the MIP-based micromotor had navigated in a solution containing 0.25 mg/mL Av-FITC target protein for (a) 0, (b) 3, (c) 5, and (d) 7 min (see SI video 3). (e) Plot showing the dependence of the estimated surface coverage on the interaction time. (B) (a–d) Time-lapse images taken after the template-imprinted microtubes had navigated for 7 min in a solution containing increasing concentrations of Av-FITC target protein: (a) 0, (b) 0.03, (c) 0.1, and (d) 0.25 mg/mL (from SI video 4). (e) Plot showing the dependence of the estimated surface coverage on the protein concentration. Fuel conditions were the same as in Figure 1. Scale bar = 20 μm. The coverages were estimated using ImageJ software and had standard deviations of <5% (n = 3).

3, which show the influence of the navigation time (in a 0.25 mg/mL target solution) upon the preconcentration efficiency (as estimated from the fluorescent coverage). The time-lapse images and video illustrate that the surface coverage increased rapidly and linearly with time up to 5 min (a–c) and then more slowly (d, e). The corresponding coverage versus time profile (e) indicates that complete fluorescent coverage was approached within 14 min, which is in agreement with Figure 2a. Overall, Figure 3A indicates that short navigation times (5–10 min) offer convenient isolation of the target protein.

The concentration dependence of the MIP micromotor–protein interaction was evaluated using a navigation time of 7 min. Figure 3B(a-d) displays images of the template-imprinted microtube taken following movement for 7 min in phosphate buffer solutions containing increasing concentrations (0–0.25 mg/mL) of Av-FITC target protein (see SI video 4). A gradual increase in the fluorescence intensity was observed as the Av-FITC concentration increased. The corresponding plot of surface coverage versus concentration [Figure 3B(e)] displays a nearly linear dependence up to 0.1 mg/mL Av-FITC and slight curvature thereafter, with 90% of the maximum coverage at 0.25 mg/mL. The fluorescence intensity can thus provide a rough quantitative estimate of the target concentration. Further analysis and regeneration of the microtransporters could be accomplished by exposure to a regeneration solution that disrupts the target–cavity interactions.[17b] Such regeneration did not compromise the movement of the micromotors.[9] MIPs have been shown to be stable even 30 days after their preparation.[19] In this work, the MIP micromotors maintained their ability to capture and transport the target protein for 7 days, after which a fresh batch was prepared and used.

The practical utility of the new microtransporter approach was illustrated by the ability of the self-propelled protein-imprinted microengines to recognize the target Av-FITC in complex unprocessed biological media such as human serum and saliva samples (Figure 4 and SI video 5). The MIP

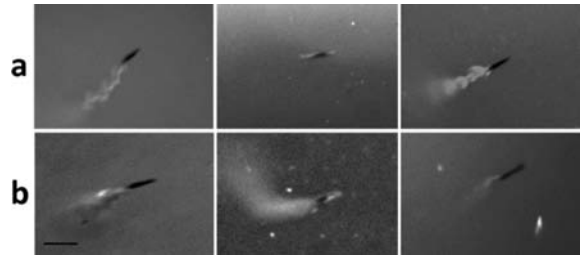

Figure 4. Capture and transport of the target protein in samples of biological fluids: (a) serum; (b) saliva. The left and middle panels show time-lapse images after the MIP-based micromotor had navigated in the samples spiked with 0.25 mg/mL Av-FITC for 0 and 7 min, respectively (see SI video 5). The right panels are images of the negative controls using a non-MIP micromotor after its 7 min navigation. Conditions were the same as in Figure 1. Untreated samples were diluted 1:4 in phosphate buffer. Scale bar = 20 μm.

microtransporters displayed efficient propulsion in these untreated biological samples and could recognize and capture a target protein. The efficient propulsion of the MIP microtransporters in the serum (Figure 4a) and saliva (Figure 4b) samples at speeds of 24.8 ± 2.9 and 20.2 ± 3.0 μm/s, respectively, allowed for their prolonged movement and direct isolation of the target protein without tedious sample processing steps. Changes in the speed can be attributed to the different viscosities and adsorption of biomolecules onto the catalytic Pt layer. The images in the middle panels of Figure 4 and the corresponding video (SI video 5) clearly illustrate the effective accumulation of the fluorescent-tagged target protein onto the MIP-based micromotors from avidin-spiked biological samples during the 7 min interaction. In contrast, no fluorescence (binding) was observed in the control experiment involving the non-MIP motor. The surface coverage was

dx.doi.org/10.1021/ja4018545 | J. Am. Chem. Soc. 2013, 135, 5336–5339

slightly lower than that observed in the phosphate buffer [67.7 ± 0.71% (serum) and 77.7 ± 0.75% (saliva) vs 90 ± 0.70%; n = 3]. Such efficient binding was not compromised by the presence of a large excess of coexisting nontarget proteins (e.g., 0.4−0.9 mg/mL total protein content in the Sigma human serum). Overall, the data in Figure 4 further support the high selectivity of the MIP nanomotor protein isolation approach and the negligible nonspecific adsorption onto the outer PEDOT/PSS layer, confirming the feasibility of the new MIP-based microtransporter concept for isolation of the target protein from complex biological fluids.

In conclusion, we have demonstrated that MIPs represent an attractive route for creating specific artificial recognition sites in synthetic self-propelled nanomachines. Tailor-made recognition sites are introduced into catalytic tubular microengine transporters as nanocavities in the outer polymer layer. The resulting template-imprinted microengines offer attractive capabilities for autonomous binding, directional transport, and enrichment of the target protein template, including "on-the-fly" isolation from raw serum and saliva matrices. While the MIP microtransporter concept was illustrated here using Av-FITC as a model protein, it could be readily extended to the selective isolation of variety of target analytes along with the construction of self-propelled microscopic and macroscopic objects,[20] offering considerable promise for diverse potential biomedical and environmental applications.

■ ASSOCIATED CONTENT

Supporting Information

Micromotor preparation, related protocols, instrumentation, reagents, additional data, and videos. This material is available free of charge via the Internet at http://pubs.acs.org.

■ AUTHOR INFORMATION

Corresponding Author

josephwang@ucsd.edu

Notes

The authors declare no competing financial interest.

■ ACKNOWLEDGMENTS

This project received support from the Defense Threat Reduction Agency−Joint Science and Technology Office for Chemical and Biological Defense (Grant HDTRA1-13-1-0002). J.O. acknowledges financial support from the Beatriu de Pinós Fellowship (Government of Catalonia). G.C. and X.F. were supported by joint-supervised Ph.D. programs with the China Scholarship Council and the Jiangsu Overseas Research & Training Program, respectively. W.G. is a Howard Hughes Medical Institute International Student Research Fellow. The authors thank G. Galicia for his assistance.

■ REFERENCES

(1) (a) Mallouk, T. E.; Sen, A. *Sci. Am.* **2009**, *300*, 72. (b) Wang, J. *ACS Nano* **2009**, *3*, 4. (c) Mirkovic, T.; Zacharia, N. S.; Scholes, G. D.; Ozin, G. A. *ACS Nano* **2010**, *4*, 1782.

(2) (a) Wang, J.; Gao, W. *ACS Nano* **2012**, *6*, 5745. (b) Pumera, M. *Nanoscale* **2010**, *2*, 1643. (c) Mei, Y. F.; Solovev, A. A.; Sanchez, S.; Schmidt, O. G. *Chem. Soc. Rev.* **2011**, *40*, 2109. (d) Sengupta, S.; Ibele, M. E.; Sen, A. *Angew. Chem., Int. Ed.* **2012**, *51*, 8434.

(3) (a) Loget, G.; Kuhn, A. *Nat. Commun.* **2011**, *2*, 535. (b) Peyer, K. E.; Torttori, S.; Qiu, F.; Zhang, L.; Nelson, B. J. *Chem.—Eur. J.* **2013**, *19*, 28.

(4) Wang, J. *Lab Chip* **2012**, *12*, 1944.

(5) Campuzano, S.; Kagan, D.; Orozco, J.; Wang, J. *Analyst* **2011**, *136*, 4621.

(6) Balasubramanian, S.; Kagan, D.; Hu, C. M.; Campuzano, S.; Lobo-Castañon, M. J.; Lim, N.; Kang, D. Y.; Zimmerman, M.; Zhang, L.; Wang, J. *Angew. Chem., Int. Ed.* **2011**, *50*, 4161.

(7) Fischer, T.; Agarwal, A.; Hess, H. *Nat. Nanotechnol.* **2009**, *4*, 162.

(8) van den Heuvel, M. G. L.; Dekker, C. *Science* **2007**, *317*, 333.

(9) Campuzano, S.; Orozco, J.; Kagan, D.; Guix, M.; Gao, W.; Sattayasamitsathit, S.; Claussen, J. C.; Merkoci, A.; Wang, J. *Nano Lett.* **2012**, *12*, 396.

(10) Orozco, J.; Campuzano, S.; Kagan, D.; Zhou, M.; Gao, W.; Wang, J. *Anal. Chem.* **2011**, *83*, 7962.

(11) Kagan, D.; Campuzano, S.; Salasubramanian, S.; Kuralay, F.; Flechsig, G. U.; Wang, J. *Nano Lett.* **2011**, *11*, 2083.

(12) (a) Wulff, G. *Angew. Chem., Int. Ed. Engl.* **1995**, *34*, 1812. (b) Mosbach, K.; Ramström, O. *Nat. Biotechnol.* **1996**, *14*, 163. (c) Chen, L.; Xu, S.; Li, J. *Chem. Soc. Rev.* **2011**, *40*, 2922.

(13) Blanco-López, M. C.; Lobo-Castañón, M. J.; Miranda-Ordieres, A. J.; Tuñón-Blanco, P. *Trends Anal. Chem.* **2004**, *23*, 36. (b) Merkoci, A.; Alegret, S. *Trends Anal. Chem.* **2002**, *21*, 717.

(14) Piletsky, S. A.; Turner, A. P. F. *Electroanalysis* **2002**, *14*, 317.

(15) (a) Kriz, D.; Ramström, O.; Svensson, A.; Mosbach, K. *Anal. Chem.* **1995**, *67*, 2142. (b) Ansell, R. J.; Ramström, O.; Mosbach, K. *Clin. Chem.* **1996**, *42*, 1506.

(16) Malitesta, C.; Losito, I.; Zambonin, P. G. *Anal. Chem.* **1999**, *71*, 1366.

(17) (a) Menaker, A.; Syritski, V.; Reut, J.; Öpik, A.; Horváth, V.; Gyurcsányi, R. E. *Adv. Mater.* **2009**, *21*, 2271. (b) Lautner, G.; Kaev, J.; Reut, J.; Öpik, A.; Rappich, J.; Syritski, V.; Gyurcsányi, R. E. *Adv. Funct. Mater.* **2011**, *21*, 591.

(18) (a) Gao, W.; Sattayasamitsathit, S.; Uygun, A.; Pei, A.; Ponedal, A.; Wang, J. *Nanoscale* **2012**, *4*, 2447. (b) Gao, W.; Sattayasamitsathit, S.; Orozco, J.; Wang, J. *J. Am. Chem. Soc.* **2011**, *133*, 11862.

(19) Bossi, A.; Piletsky, S.; Piletska, E.; Giorgio, P.; Turner, A. *Anal. Chem.* **2001**, *73*, 5281.

(20) Zhao, G.; Pumera, M. *Chem.—Asian J.* **2012**, *7*, 1994.